JOURNAL OF THERMOPHYSICS AND HEAT TRANSFER
Vol. 25, No. 3, July–September 2011

Technical Notes

Measurement of Density Distribution over a Hemisphere in Ballistic Range

Satoshi Nonaka*
Japan Aerospace Exploration Agency, Sagamihara 252-5210, Japan
Tokitada Hashimoto†
Saga University, Saga 840-8502, Japan
Michiko Furudate‡
Chungnam National University, Daejeon 305-764, Republic of Korea
and
Kazuyoshi Takayama§
Tohoku University, Sendai 980-8577, Japan

DOI: 10.2514/1.51123

Nomenclature

f	=	basis function
L	=	optical beam length past test section, m
M	=	Mach number
R	=	radius of sphere, m
T	=	translational temperature, K
T_v	=	vibrational temperature, K
β	=	dimensionless constant related to refraction index
Δ_s	=	shock standoff distance along the stagnation streamline, m
ρ	=	density, kg/m^3
ρ_{ref}	=	reference density, kg/m^3
ρ_s	=	standard density, kg/m^3

I. Introduction

WHEN a space vehicle flies in the atmosphere at hypersonic speed, temperature behind the shock wave that develops over the vehicle becomes so high that the so-called real-gas phenomena become dominant. The real-gas phenomena, such as vibrational excitation, dissociation, and ionization reaction of chemical species, usually absorb heat of the gas and thereby reduce the temperature in the shock layer. The reduction of temperature results in increase of density of the gas, and the shock layer thickness is consequently reduced. This suggests that the pressure distributions over the space vehicle in the real-gas flow regime are significantly different from those in the ideal-gas predictions. Therefore, when one designs hypersonic vehicles, the real-gas phenomena need to be taken into account in order to predict aerodynamic characteristic accurately.

To accomplish accurate predictions of a nonequilibrium flowfield, computational fluid dynamics (CFD) codes for hypersonic vehicle designs should be validated by using reliable experimental data in the hypersonic region. To obtain the reliable data for the CFD validations, shock standoff distance and shock shape over sphere have been measured in a ballistic range [1,2]. Those results were obtained in the intermediate hypersonic regime between 2.5 and 4 km/s and were used to validate a CFD code using a two-temperature mode [3,4]. In ballistic ranges, the test model is accelerated to hypersonic velocities in a quiescent test gas so that the initial conditions and the composition of test gases are correctly controlled. In this manner, hypersonic flights achieved in a ballistic range are able to produce appropriate reliable data for CFD validation.

Since shock shapes over simple geometries are sensitive to the real-gas effects, they can be one of the most appropriate reference quantities for the CFD validations [3]. The change of shock shape is caused by the change of the density distribution in the shock layer. In thermochemical nonequilibrium state over a sphere, the density along the stagnation streamline increases gradually in the shock layer, due to the vibrational relaxation of molecules. Therefore, the density in the shock layer is also an important parameter for the evaluation of the real-gas effects. In the present study, the density distribution over a hemisphere is measured in a ballistic range in the intermediate hypersonic regime. The obtained data are compared with numerical simulations for evaluations of real-gas effects.

The holographic visualization is advantageous for the quantitative data acquisition of density distribution behind a shock wave [5]. Fringes in infinite fringe holographic interferometry correspond to isopycnics. So the fringe distribution can readily validate numerically reproduced isopycnic [6,7]. Since the sensitivity of the interferogram is proportional to the initial pressure and the length of light path through the test section, the spatial resolution is reduced if the initial density is low or the length of light pass is short. Under the conditions to produce the thermochemical nonequilibrium flow over a hemispherical model in the ballistic range experiment, the initial pressure is required to be relatively low. In addition to this, the effective path length of the object beam through the shock layer over the small model is short. Therefore, few fringes are created on the interferogram. On the other hand, the finite fringe holographic interferometry is reasonable in such conditions of low pressure and short light-path length, because fringes can be sensitively shifted in low pressure, and the special resolution can be increased by adjusting the fringe number. The density field data can be quantitatively obtained from fringe analysis by means of Fourier fringe analysis [8,9]. The obtained density distribution in the shock layer is expected to be reasonable data for the CFD validations. In the present study of measuring density distribution in the shock layer, the finite fringes were created over a hemispherical model by double-exposure finite fringe holographic interferometry.

II. Test Facilities and Conditions

A. Ballistic Range

The experiment was conducted in the ballistic range in the Shock Wave Research Center of the Institute of Fluid Science, Tohoku University. Figure 1 shows a schematic of the ballistic range. This facility has been constructed as a two-stage light gas gun consisting of a powder chamber, a 60-mm-i.d. pump tube of 3 m in length, a high-pressure coupling, a 30-mm-i.d. launch tube of 4 m in length, and a test chamber. The test chamber is 700 mm in i.d. and 1400 mm in length. The inside wall of the test chamber is cleaned after each shot in order to keep the contamination level in the chamber very low.

Received 11 June 2010; revision received 1 March 2011; accepted for publication 3 March 2011.

*Assistant Professor, Institute of Space and Astronautical Science, 3-1-1 Yoshinodai, Kanagawa. Member AIAA.
†Assistant Professor, Department of Mechanical Engineering, 1 Honjyo. Member AIAA.
‡Lecturer, Department of Mechatronics Engineering, 220 Gung-dong, Yuseong-gu. Member AIAA.
§Professor, Institute of Fluid Science, 2-1-1 Katahira, Aoba, Miyagi. Member AIAA.

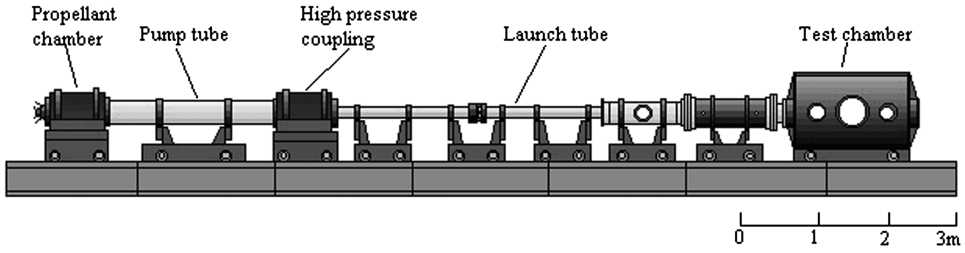

Fig. 1 Ballistic range in Tohoku University.

The operation of the ballistic range is as follows. A high-density polyethylene piston is accelerated along the pump tube by a high-pressure gas generated by the combustion of smokeless powder in the propellant chamber. The piston compresses a light gas, such as hydrogen or helium, which fills the pump tube. The resulting high-pressure light gas ruptures the steel diaphragm inserted between the pump tube and the high-pressure coupling, and accelerates the hemisphere model along the launch tube. The model is launched into the test chamber and eventually terminates on a steel bumper in the test chamber. The velocity of the model is measured by the time of flight of the model between two laser beams placed at a 800 mm distance apart in the test section.

B. Holographic Interferometry

Holographic interferometry was used for the measurement of density distribution over a 15-mm-nose-radius hemisphere. Figure 2 shows the optical arrangement of double-exposure holographic interferometry. The light source is a pulse ruby laser (Apollo Laser Company, Ltd., 2HD) with wavelength of 694–3 nm, a 25 ns pulse duration, and 2 J energy. This optical arrangement is basically similar to a conventional shadowgraph optic except that the ruby laser is split into an object beam and a reference beam by using a beam splitter. A pair of paraboloidal mirrors of 300 mm in diameter and 3 m in focal length was used to collimate the object beam. The reference beam is expanded by a plane-concave lens and collimated to illustrate a holographic film.

In infinite fringe holographic interferometry, no optical arrangements are moved during the first and second exposures, and the fringes correspond to isopycnic lines. On the other hand, the intersection angle between the object and reference beam is shifted by tilting the collimating lens of reference beam in finite fringe holographic interferometry. In this study, the density distribution over the hemisphere model is measured by the finite fringe holographic interferometry.

The hologram was constricted on an Agfa-Gevaert 10E75 100 × 125 mm sheet film. The hologram was reconstructed by illuminating the hologram with an argon–ion laser of 514.5 nm wavelength. The reconstructed interferograms were recorded on a Neopan SS 100 × 125 mm sheet film.

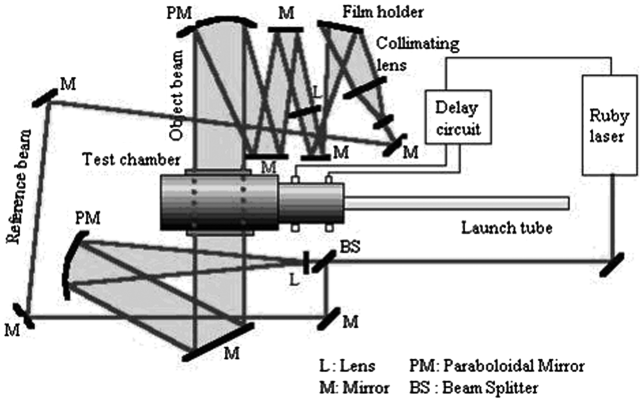

Fig. 2 Optical arrangement of finite fringe holographic interferometry.

C. Test Conditions

Test conditions were selected from the result of a shock standoff distance measurement in [3] to generate nonequilibrium flow over a moving sphere. The selected binary scaling parameter ρR is 8.5×10^{-4} kg/m^2. The corresponding initial pressure for the 15-mm-nose-radius sphere was 5.1×10^3 Pa. The model was made of AZ-31-F magnesium alloy and machined in the shape of a hemisphere cylinder with a nose radius of 15 mm. The model weight was 18.7 g, and its muzzle velocity was 2.53 km/s.

Smokeless powder of 80 g in weight was used to propel a 1550 g high-density polyethylene piston. Diaphragms inserted between the powder chamber and the high-pressure coupling were made of 1.0-mm-thick stainless steel and 2.5-mm-thick steel, respectively. The helium pressure in the pump tube was 7.4×10^5 Pa and the initial temperature in dry air in the test chamber was 293 K.

III. Analysis of Finite Fringe Interferogram

The obtained finite fringe interferograms of two-dimensional and axisymmetric shock wave flows were analyzed by using the method of Houwing et al. [8,9]. The density field data were produced by Fourier transform fringe analysis and an Abel inversion method. The method involves the following steps [10]:

1) Scan the finite fringe interferograms and apply a two-dimensional Fourier transformation to the fringe spacings.

2) Apply a filter operation in the Fourier transform plane.

3) Perform a frequency shift in the Fourier transform plane so that the data are located around zero frequency.

4) Produce a two-dimensional inverse Fourier transform of the filtered and frequency-shifted Fourier transform.

5) Determine the phase by evaluating the arctangent of the ratio of the imaginary and real parts of the inverse transform.

6) Unwrap the phase by adding multiples of 2π where required.

7) Remove any residual background phase.

The density distribution is obtained from phase data produced by these steps of the fringe analysis. Using the Abel inversion method, the density in axisymmetric flows is given by

$$\rho(r,z) = \frac{\rho_s}{\beta} f(r,z) + \rho_{\text{ref}}$$

where values for β and ρ_s for air used in the present study are available in [11]. The function $f(r,z)$ is equal to a linear combination of basis function in a cylindrical polar coordinate system [9].

IV. Numerical Method

In the present study, thermochemical nonequilibrium flow over a hemisphere is calculated by using a numerical code developed in [3]. The governing equations are the axisymmetric Navier–Stokes equations, consisting of global mass conservation, species mass conservation equation, momentum conservation equation, total energy conservation equation, and vibrational–electronic conservation equation of motion.

Five neutral species, O_2, N_2, O, N, and NO are considered. By using the idea of elementary conservation in which the ratio of oxygen and nitrogen atoms is kept constant everywhere, two-species conservation equations can be removed from the set of governing equations [12]. This assumption is valid even for viscous flow calculations if the net diffusion velocities for the oxygen and nitrogen

atoms are identical, which is well satisfied in air. In this study, these three species conservation equations for N, O, and NO are solved.

Park's [13] two-temperature model is employed to determine the chemical reaction rate coefficients. According to this model, the rate coefficients for dissociation reactions due to two-body collisions are a function of the geometric-averaged temperature between translational–rotational temperature T and vibrational–electronic temperature T_v, $\sqrt{TT_v}$ [14]. The translational–vibrational energy relaxations are calculated by the Landau–Teller equation.

The numerical scheme is based on the cell-vertex finite volume method [15], and a structured-mesh system is employed. The convective numerical flux is calculated by the AUSM-DV upwind scheme. The dependent variables are interpolated by the MUSCL approach in order to improve special accuracy. The two-level second-order explicit Runge–Kutta method is used for time integration. For the convergence acceleration, the local time-stepping method is used.

V. Results and Discussions

A. Interferogram

Figure 3 shows the obtained finite fringe holographic interferogram for the flow over the hemisphere model. The fringe shift can be seen across the bow shock wave. Immediately behind the shock, the optical path length through the shock layer is nearly zero, and continuously increases with distance toward downstream. From this interferogram, the shock standoff distance normalized by nose radius, Δ_s/R, is determined to be $0.131 \pm 0.5\%$. Figure 4 shows the present value of Δ_s/R and the previous data obtained in [1]. The upper solid curve designates the analytical results for an ideal gas of $\gamma = 1.4$, which corresponds to the case of $\rho R = 0$. The two lower lines give the predicted values of Δ_s/R at two different ambient pressures in equilibrium condition, which corresponds to the value of $\rho R = \infty$. When compared with the data in [1], the present result indicates that the flow in the shock layer is sufficiently non-equilibrium.

B. Density Distribution

The image data from the interferogram was stored on a workstation by using a high-resolution scanner, and then it was analyzed as described in Sec. III. Figure 5 shows the density distribution over the hemisphere obtained from the finite fringe interferogram and the nonequilibrium flow calculation. It is noted that the shock shape and the density contour obtained in the experiment agree well with those in the calculated result. The experimental and the calculated density profiles along the stagnation streamline are shown in Fig. 6, and the density profiles along the streamwise line at $r = 0.010$ and 0.015 m are shown in Figs. 7a and 7b, respectively. The measured values of the density ratio along the stagnation streamline shown in Fig. 6 are

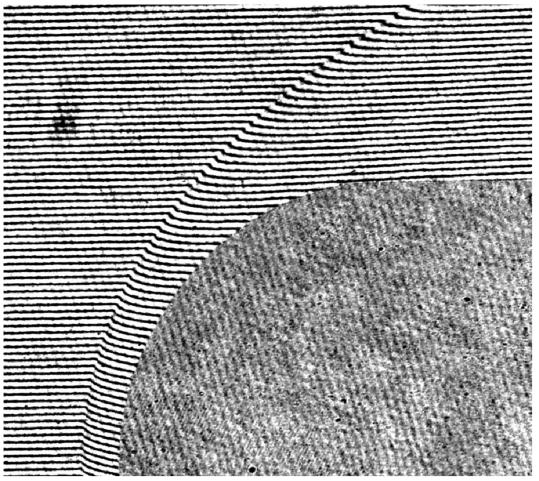

Fig. 3 Finite fringe holographic interferogram over a hemisphere model at 2.53 km/s.

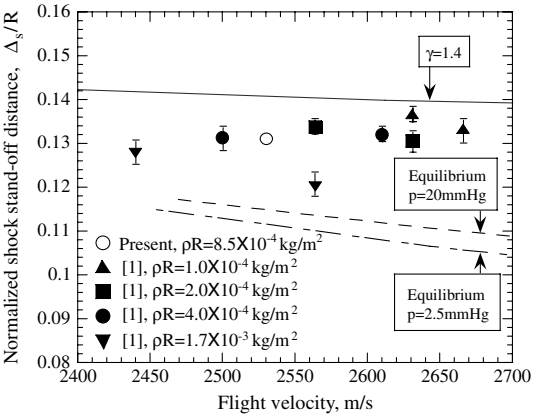

Fig. 4 Normalized shock standoff distance for sphere.

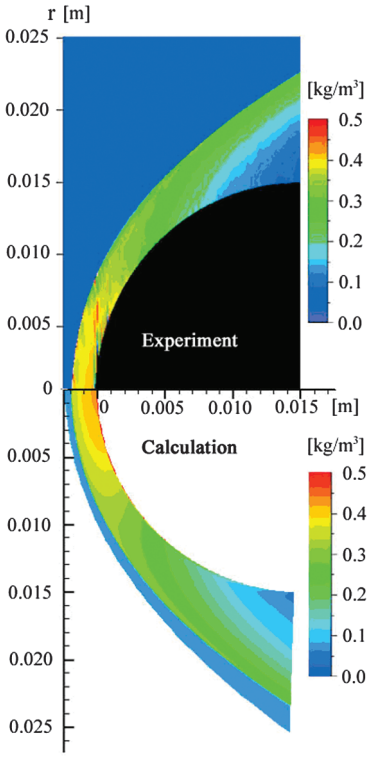

Fig. 5 Density distribution over a hemisphere in experiment and calculation.

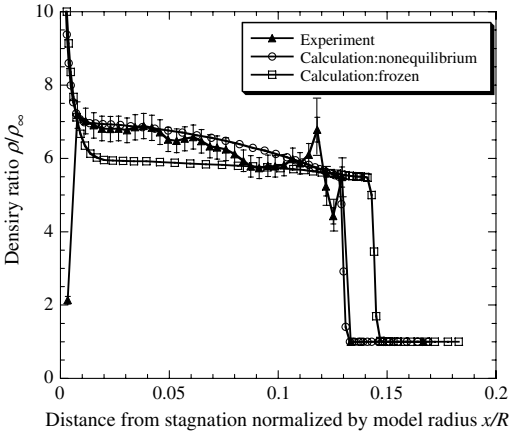

Fig. 6 Density profiles along stagnation streamline in experiment and calculations.

Table 1 Density ratio along stagnation stream line in experimental measurements shown in Fig. 6.

Normalized distance from body surface	Density ratio	Normalized distance from body surface	Density ratio
0.167	1.00	0.069	6.33
0.133	1.00	0.065	6.47
0.129	5.49	0.061	6.58
0.125	4.43	0.057	6.53
0.122	5.23	0.053	6.48
0.118	6.78	0.050	6.52
0.114	6.10	0.046	6.72
0.110	5.87	0.042	6.83
0.107	5.98	0.038	6.88
0.103	5.82	0.034	6.85
0.099	5.78	0.031	6.77
0.095	5.80	0.027	6.82
0.091	5.73	0.023	6.80
0.087	5.78	0.019	6.82
0.084	5.93	0.015	6.90
0.080	6.12	0.012	7.02
0.076	6.25	0.008	7.18
0.072	6.30	0.003	2.13

summarized in Table 1. To evaluate the real-gas effects on density distribution, the density profiles obtained from the experiment and the nonequilibrium calculation are compared with the calculation assuming a frozen flow. The frozen calculation was carried out by using the same computational code as the nonequilibrium calculation, but the chemical reaction and vibrational excitation rates were assumed to be zero. The abscissa in Figs. 6 and 7 are distance from the body surface normalized by nose radius, and the ordinate is the density normalized by the initial density.

In axisymmetric flows, the optical path length through the shock wave is nearly zero at the shock front along the stagnation streamline because it is the apex of a bow shock. The fringe shift in the interferogram occurs because of a phase shift of the object beam passing through the shock layer. This means that the density jump at the shock front along the stagnation streamline cannot be identified merely from the fringe analysis. Therefore, this density jump in the axisymmetric fringe analysis must be theoretically or numerically estimated. The state immediately behind a shock wave is considered to be nearly thermochemically frozen. In this case, the density ratio across the shock wave is estimated from the shock relation,

$$\frac{\rho_2}{\rho_1} = \frac{(\gamma+1)M^2}{(\gamma-1)M^2+2}$$

where $M = 7.37$ and $\gamma = 1.4$. As a result, the density ratio at the shock wave along the stagnation streamline is determined as to be 5.49.

At the shock front, the density fluctuations are recognized. These fluctuations may be due to errors in the density estimation immediately behind a bow shock wave. Immediately behind a shock, the object beam passing through the shock layer is extremely short, that is, errors in estimating fringe shift in fringe analysis becomes large. Errors in the density estimation immediately behind a shock are expected to be below $\pm 10\%$, and errors in the other area in the shock layer are expected to be below $\pm 5\%$. These errors also account for the model movement during a laser pulse.

It is recognized that the density profiles along the stagnation streamline in Fig. 6 obtained in the experiment and in the

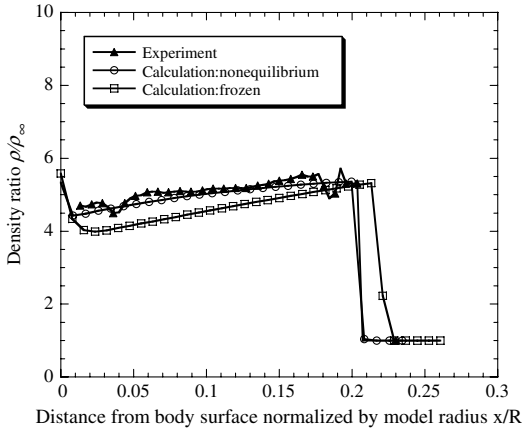

a) r = 0.010m

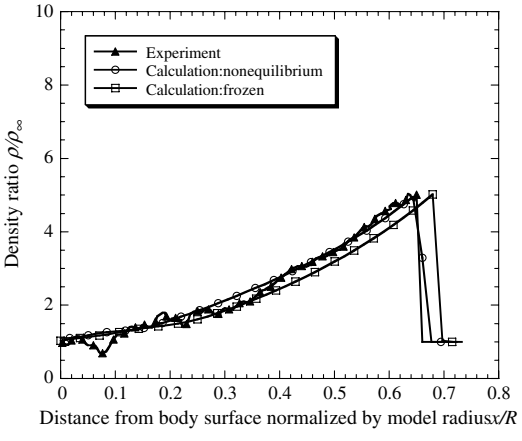

b) r = 0.015m

Fig. 7 Density profiles along streamwise lines in experiment and calculations.

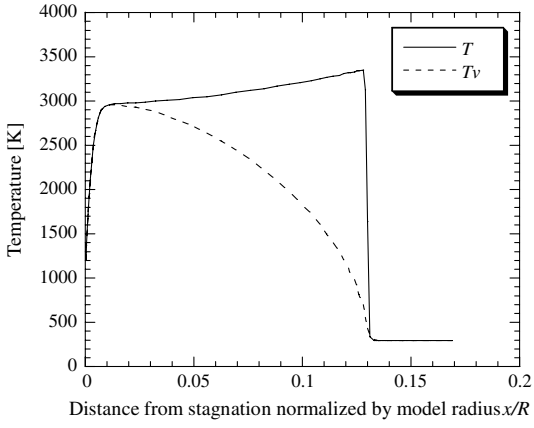

a) Temperature profile

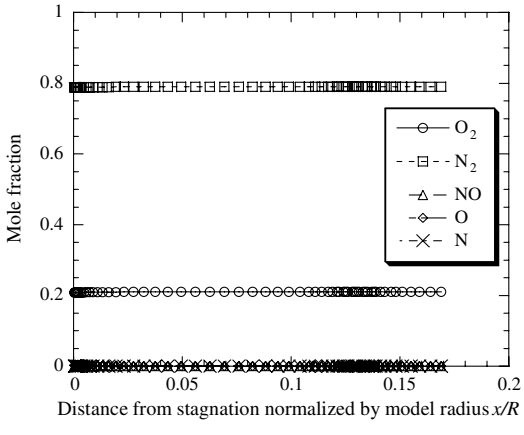

b) Mole fraction profile

Fig. 8 Temperature and mole fraction along stagnation streamline in nonequilibrium calculation.

nonequilibrium calculation are in good agreement with each other. In particular, the calculated shock standoff distance normalized by the nose radius is 0.130, and agrees well with the experimental value. These density profiles increase gradually toward the body surface while that of the frozen flow calculation shows almost constant density in the shock layer. The frozen density ratio along the stagnation streamline levels off to be nearly 6, whereas the experimental density ratio is found to be about 7 and tends to increase toward the body surface. This density increase may be due to the real-gas effects. The high temperature behind the shock front excites vibrational modes of the O_2 and N_2 molecules, and then decreases. As a result of it, the density increases. In Fig. 7, it is also recognized that the density profiles obtained in the experiment and in the nonequilibrium calculation are in good agreement with each other.

Figures 8a and 8b show nonequilibrium calculation results of the temperature and the species mole fractions profiles along the stagnation streamline, respectively. In Fig. 8a, the vibrational temperature T_v reaches the translational temperature T at the edge of boundary layer. Chemical reactions are not dominant as seen in Fig. 8b. That is, the flowfield is in thermal nonequilibrium and chemically frozen.

VI. Conclusions

By using finite fringe holographic interferometry, the density distribution over a hemisphere at 2.53 km/s has been measured in a ballistic range and the following conclusions were drawn. The experimental density profiles were well reproduced by the nonequilibrium calculation using the two-temperature model. From the calculated result, the present flowfield in the shock layer was found to be in a thermal nonequilibrium state. The density increase from the frozen value due to the real-gas effects was clearly recognized. The finite fringe interferometry can quantitatively determine the density including the dominant real-gas effect, even in the intermediate hypersonic region. It was indicated that this technique is useful to provide a database to validate numerical codes for nonequilibrium hypersonic flow.

Acknowledgments

The authors wish to thank H. Mizuno of the Japan Aerospace Exploration Agency and O. Onodera, H. Ojima, and T. Ogawa of the Shock Wave Research Center at Tohoku University for their help in conducting the present experiments. The authors would like to express thanks to A. F. P. Houwing of Australia National University for his help in analysis of finite fringe interferogram. The authors would like to thank K. Sawada of Tohoku University for his help in conducting the present calculations.

References

[1] Nonaka, S., Mizuno, H., Takayama, H., and Park, C., "Measurement of Shock Standoff Distance for Sphere in Ballistic Range," *Journal of Thermophysics and Heat Transfer*, Vol. 14, No. 2, 2000, pp. 225–229. doi:10.2514/2.6512

[2] Nonaka, S., Mizuno, H., and Takayama, K., "Ballistic Range Measurement of Shock Shapes in Intermediate Hypersonic Regime," AIAA Paper 99-1025, 1999.

[3] Furudate, M., Nonaka, S., and Sawada, K., "Behavior of Two-Temperature Model in Intermediate Hypersonic Regime," *Journal of Thermophysics and Heat Transfer*, Vol. 13, No. 4, 1999, pp. 424–430. doi:10.2514/2.6480

[4] Furudate, M., Nonaka, S., and Sawada, K., "Calculation of Shock Shapes over Sharp Cone in Intermediate Hypersonic Air Flow," *Journal of Thermophysics and Heat Transfer*, Vol. 17, No. 2, 2003, pp. 250–258. doi:10.2514/2.6758

[5] Takayama, K., "Application of Holographic Interferometry to Shock Wave Research," *Proceedings of SPIE: The International Society for Optical Engineering*, Vol. 398, 1983, pp. 174–180.

[6] Babinsky, H., and Takayama, K., "CFD Validation Strategies for Compressible Flow Using Interferometry," AIAA Paper 96-0438, 1996.

[7] Abe, A., Ojima, H., Ogawa, T., Babinsky, H., and Takayama, K., "Animated Display of Sequential Holographic Interferograms of Shock Wave/Vortex Propagation," *Proceedings of the International Symposium on Shock Waves*, 1999.

[8] Houwing, A. F. P., Takayama, K., Jiang, Z., Sun, M., Yada, K., and Mitobe, H., "Interferometric Measurement of Density in Nonstationary Shock Wave Reflection Flow and Comparison with CFD," *Shock Waves*, Vol. 14, Nos. 1–2, 2005, pp. 11–19. doi:10.1007/s00193-005-0243-z

[9] Houwing, A. F. P., Takayama, K., Jiang, Z., Hashimoto, T., Koremoto, K., Mitobe, H., and Gaston, M. J., "Abel Inversion of Axially-Symmetric Shock Wave Flows," *Shock Waves*, Vol. 14, Nos. 1–2, 2005, pp. 21–28. doi:10.1007/s00193-005-0244-y

[10] Bone, D. J., "Fourier Fringe Analysis—The Two-Dimensional Phase Unwrapping Problem," *Applied Optics*, Vol. 30, 1991, pp. 3627–3632. doi:10.1364/AO.30.003627

[11] Liepmann, H. W., and Roshko, A., "Elements of Gasdynamics," Wiley, New York, 1957.

[12] Park, C., "Nonequilibrium Hypersonic Aerothermodynamics," Wiley, New York, 1990.

[13] Park, C., "A Review of Reaction Rates in High Temperature Air," AIAA Paper 89-1740, 1989.

[14] Park, C., "Assessment of Two-Temperature Kinetic Model for Ionizing Air," *Journal of Thermophysics and Heat Transfer*, Vol. 3, 1989, pp. 233–244. doi:10.2514/3.28771

[15] Niizuma, K., and Sawada, K., "Nonequilibrium Flow Computation for the Space Shuttle Nose Using Unstructured Meshes," AIAA Paper 97-2548, 1997.